

The a_1 in τ decay

Nathan Isgur, Colin Morningstar, and Cathy Reader

Department of Physics, University of Toronto, Toronto, Canada M5S 1A7

(Received 15 June 1988; revised manuscript received 11 October 1988)

The decay $\tau \rightarrow \nu_\tau \pi \pi \pi$ provides a potentially powerful means of observing the axial-vector isovector state expected in the region of 1.2 GeV. Extraction of the properties of this resonance is, however, complicated by its broad width. We examine the problems of studying such a resonance, especially the model dependence of its deduced mass and width. Within a clearly defined and well-tested model we find $m_{a_1} = 1220 \pm 15$ MeV and $\Gamma_{a_1} = 420 \pm 40$ MeV.

I. INTRODUCTION

Twenty-five years after the birth of the quark model, light-meson spectroscopy is in a deplorable state. In particular, aside from the tensor mesons, our knowledge of the simple $L=1$ orbitally excited states is extremely poor. Of the 12 states of the ${}^3P_1(J^{PC_n}=1^{++})$, ${}^1P_1(J^{PC_n}=1^{+-})$, and ${}^3P_0(J^{PC_n}=0^{++})$ nonets, one can reasonably argue¹ that only six [the $f_1(1285)$, $b_1(1235)$, $h_1(1190)$, $K_1(1280)$, $K_1(1400)$, and $K_0^*(1350)$] are satisfactorily understood, and even these six states are not without their problems.

This paper is concerned with new information on the axial-vector isovector (a_1) state obtained from recent measurements of the decay $\tau \rightarrow \nu_\tau \pi \pi \pi$. The structure of the three-pion final states in this reaction is a potentially powerful tool for studying the a_1 . Indeed, were the a_1 a reasonably narrow resonance, the extraction of its properties from this reaction would be almost trivial: the $\tau \rightarrow \nu_\tau \pi \pi \pi$ transition scans in $m_{3\pi}$ from $3m_\pi$ to m_τ with a known probe, the axial-vector current. Problems arise, however, from ambiguities which are present in the treatment of what is actually a broad resonance. One reflection of these problems is the wide range of masses

and widths which have been extracted from such data²⁻⁵ (see Table I).

The properties of the a_1 were first studied in hadronic reactions. These studies^{6,7} were complicated not only by the broad width of the a_1 , but also by the presence of strong backgrounds, especially the diffractive "Deck effect."⁸ The standard values of the a_1 parameters quoted by the Particle Data Group⁹ are based mainly on these analyses (see Table I). The discrepancy between the properties of the a_1 deduced from τ decay and the hadronic reactions is obviously another cause for concern. This discrepancy has been studied recently by Bowler¹⁰ who, based on an observation in Ref. 3, found that (1) the different results quoted by Refs. 2, 3, and 4 (Ref. 5 was published later) were due primarily to their differing treatments of off-shell effects (which are important given the large a_1 width) and not to differences in their data and (2) that a fit to the data allowing for unknown mass dependence of the decay amplitudes off resonance gave an a_1 mass, but perhaps not a width, from τ decay consistent with that from the hadronic experiments. He also showed that a similar mass dependence was indicated by fits to the ρ -dominated processes $e^+e^- \rightarrow \pi^+\pi^-$ and $\tau \rightarrow \nu_\tau \pi \pi^0$. The result is a very strong phenomenological

TABLE I. Masses and widths of the a_1 .

Source	Mass (MeV)	Width (MeV)
DELCO (τ decay) ^a	1056±20±15	476 ⁺¹³² ₋₁₂₀ ±54
Mark II (τ decay) ^b	1194±14±10	462±56±30
Argus (τ decay) ^c	1046±11	521±27
MAC (τ decay) ^d	1166±18±11	405±75±25
$\pi^- p \rightarrow \pi^- \pi^+ \pi^- p$ ^e	1280±30	300±50
$\pi^- p \rightarrow \pi^- \pi^0 \pi^+ n$ ^f	1240±80	380±100
PDG ^g	1275±28	316±45
Bowler ^h	1235±40	400±100
This work	1220±15	420±40

^aReference 2.

^bReference 3.

^cReference 4.

^dReference 5.

^eReference 6.

^fReference 7.

^gReference 9.

^hReference 10.

case that there is no major discrepancy between the τ and hadronic data.

Following the observation made in Ref. 3 of the crucial role mass dependence plays in extracting the properties of the a_1 from τ decay, we began this work with the aim of deducing this mass dependence from theory. Our results and their interpretation are roughly consistent with Bowler's. Thus, in one sense, this work may be considered a justification for the spirit of his parametrization of the $\tau \rightarrow \nu_\tau a_1$ mass dependence. However, we also determine, within the context of the assumptions we make, the full mass dependences of the $\tau \rightarrow \nu_\tau \pi\pi\pi$ amplitude and their physical origins. To the extent that our assumptions can be trusted (a subject we address below), this eliminates a large part of the uncertainty in deducing the a_1 's parameters. We also expose several minor errors that have been made in previous analyses of the $\tau \rightarrow \nu_\tau \pi\pi\pi$ process. One of these errors concerns the treatment of the two possible (on-shell) $a_1 \rightarrow \rho\pi$ couplings. We find no good reason for the usual neglect of one of these two couplings and, on adding it with the strength predicted by the flux-tube-breaking model we find an improvement in the description of the Dalitz-plot projections. Another is related to the treatment of off-mass-shell propagators and vertices which can lead in general to nonresonant amplitudes, including ones with new J^{PC} quantum numbers. In addition we study effects in $\tau \rightarrow \nu_\tau \pi\pi\pi$ due to the radial excitation of the pion.

II. MODELS AND METHODS

A. Time-ordered perturbation theory

If hadrons were pointlike particles, there would be no problem (at least in principle) in treating the decay $\tau \rightarrow \nu_\tau \pi\pi\pi$ with arbitrary precision in terms of the hadronic fields. Since hadrons are instead composite objects, one encounters difficulties in using them as effective degrees of freedom. Perhaps foremost among these problems are those which emerge when one tries to perform covariant perturbation theory.

A Feynman diagram is a sum of time-ordered graphs, some of which involve particles, and others antiparticles, propagating forward in time. A crucial requirement for the graphs of time-ordered perturbation theory to combine into a covariant graph is that the elementary vertices be pointlike so that, for example, $e^- \rightarrow e^- \gamma$ and $e^+ e^- \rightarrow \gamma$ have the same strength. Hadrons do not possess this property. Figure 1 illustrates this point in the context of the problem at hand. The $a_1 \rightarrow \rho\pi$ vertex of Fig. 1(a) is something that can be measured on shell; it can also be computed with a modest degree of reliability in various models since it involves the creation of only a single quark-antiquark pair. The creation of $a_1 \rho\pi$ by the strong interaction from the vacuum, the amplitude at the heart of the Z graph of Fig. 1(b), is not easily measurable nor is it an amplitude one expects to match in strength the $a_1 \rightarrow \rho\pi$ decay amplitude since it involves the creation from the vacuum of three $q\bar{q}$ pairs. In fact, there are cases, such as $\gamma p \rightarrow p$ versus $\gamma \rightarrow p\bar{p}$ at low energy, where one knows from direct measurements that the Z-graph

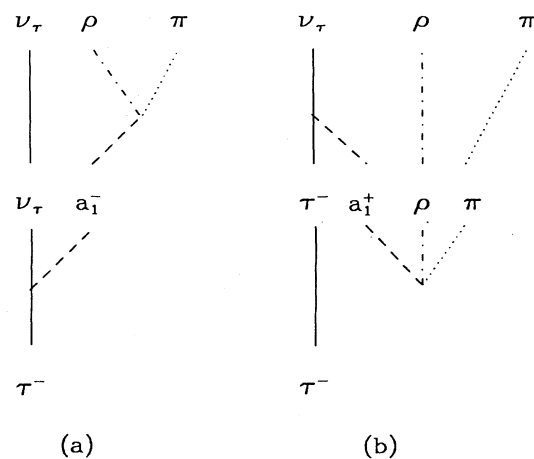


FIG. 1. Two time-ordered graphs which would combine to form a covariant Feynman graph for pointlike particles: (a) strong decay following the weak creation of a_1^- and (b) an $a_1 \rho\pi$ "vacuum fluctuation" followed by annihilation of a_1^+ .

vertex is suppressed.

This observation creates a dilemma—one can either have a manifestly covariant calculation containing a piece of manifestly incorrect physics or one can have a calculation which uses the correct vertices but is not manifestly covariant. For narrow resonances, this dilemma is not a serious one because each second-order Z graph such as Fig. 1(b), representing a fraction $|(E-M)/2E|$ of the total Feynman graph for pointlike coupling, is already unimportant since in the resonance peak $|(E-M)/2E| \approx \Gamma/2M \ll 1$. However, the a_1 populates the 3π mass spectrum over essentially its entire kinematic range. Thus, $|(E-M)/2E|$ can be substantial and the standard use of covariant perturbation theory is probably unjustified.

As a consequence of this, and given our more or less complete ignorance of everything about the Z-graph vertices except that they seem likely to be suppressed,¹¹ we *ideally* would like to keep in our analysis only the naively time-ordered graphs, i.e., the non-Z graphs such as Fig. 1(a). They are the graphs which resonate while the Z graphs provide a smooth nonresonant "background." *Realistically*, however, the convenience of the covariant approach is difficult to sacrifice, especially when dealing with four-body phase space. We describe our alternative method of decoupling the suspect Z-graph "backgrounds" from the resonance below.

B. Mass dependence of amplitudes

The conceptual separation of the resonant (and presumably dominant) time-ordered graphs from non-resonant effects, in addition to being important for the reasons just given, has other advantages. One is that their off-shell behavior is (more or less) completely calculable. This eliminates one of the most serious uncertain-

ties in studying the a_1 in τ decay. Another is that all of the allowed $a_1 \rightarrow \rho\pi$ and $\rho \rightarrow \pi\pi$ couplings for the resonant graphs can be treated. This contrasts with the covariant graph procedure in which most of the allowed

couplings are eliminated without full justification.

Consider the Feynman graphs of Fig. 2. The most general $a_1 \rightarrow \rho\pi$ vertex factor that may appear in such a graph is

$$\Gamma^{\mu\nu}(a_1 \rightarrow \rho\pi) \propto f_1 g^{\mu\nu} + f_2 (p_\rho - p_\pi)^\mu (p_{a_1} + p_\pi)^\nu + f_3 (p_\rho + p_\pi)^\mu (p_{a_1} + p_\pi)^\nu + f_4 (p_\rho - p_\pi)^\mu (p_{a_1} - p_\pi)^\nu + f_5 (p_\rho + p_\pi)^\mu (p_{a_1} - p_\pi)^\nu, \quad (1)$$

where $p_{a_1} = p_\pi + p_\rho$ and the f_i 's are form factors which can depend on $p_{a_1}^2$ and p_ρ^2 . In the usual treatment, only f_1 and f_2 are allowed to be nonzero.¹²⁻¹⁶ In general, this is correct *only* if all of the participants in the decay $a_1 \rightarrow \rho\pi$ are on-mass shell since then $\epsilon_{a_1} \cdot p_{a_1} = \epsilon_\rho \cdot p_\rho = 0$, where ϵ_{a_1} and ϵ_ρ are polarization vectors. Similarly, the general $\rho \rightarrow \pi\pi$ vertex factor may be written

$$\Gamma^\mu(\rho \rightarrow \pi_1\pi_2) \propto g_1 (p_{\pi_1} - p_{\pi_2})^\mu + g_2 (p_{\pi_1} + p_{\pi_2})^\mu, \quad (2)$$

and the usual neglect of g_2 is valid only when the ρ is on-mass shell. Finally, one must also allow for mass dependence in the weak $W \rightarrow a_1$ vertex:

$$\Gamma^{\mu\sigma}(W \rightarrow a_1) = -i f_{a_1} (p_{a_1}^2) g^{\mu\sigma}. \quad (3)$$

We thus see that the unknown off-shell behavior of these graphs can be problematical. Not only does one not know the dependence of f_{a_1} on $p_{a_1}^2$ (the dependence associated with Bowler's parametrization¹⁰ of the off-shell behavior), but one also knows neither the off-shell dependence of f_1, f_2 , and g_1 nor the functions f_3, f_4, f_5 , and g_2 which can play a role off shell.

There is a closely related problem in taking the vector propagators for either the a_1 or ρ off shell (see Appendix A). This propagator is sometimes taken to be (ignoring decay channels for illustrative purposes)

$$-i\tilde{P}^{\mu\nu}(k) = \frac{-g^{\mu\nu} + k^\mu k^\nu / k^2}{k^2 - m^2 + i\epsilon} \quad (4)$$

instead of

$$-iP^{\mu\nu}(k) = \frac{-g^{\mu\nu} + k^\mu k^\nu / m^2}{k^2 - m^2 + i\epsilon}. \quad (5)$$

These two propagators only differ significantly far off shell so that the choice between them corresponds to yet another difficulty that does not arise for narrow resonances. For hadrons treated as elementary fields, the latter propagator should be used although it often is not. Note, for example, that if \tilde{P} were used for the W boson, $\pi \rightarrow \mu\nu$ would be forbidden.

Given all of these problems, one might despair of computing the correct mass dependence in $\tau \rightarrow \nu_\tau \pi\pi\pi$. However, almost all of the ambiguities we have just discussed are associated with the nonresonant background which according to the discussion of time-ordered perturbation theory made above is an unknown common to all analyses anyway. To see this in a simplified context, consider the production of $\pi^+\pi^-$ via the ρ in $e^+e^- \rightarrow \pi^+\pi^-$. To compute the amplitude for the graph analogous to Fig. 1(a) in the e^+e^- center-of-momentum frame one need only know for *physical states* the two matrix elements:

$$\langle \rho(\mathbf{0}, s_\rho) | j_{em}^\mu(0) | 0 \rangle \propto f_\rho \epsilon_\rho^{*\mu} \quad (6)$$

and

$$\langle \pi^+(\mathbf{p})\pi^-(\mathbf{-p}) | H_{sb}(0) | \rho(\mathbf{0}, s_\rho) \rangle \propto g_1 \epsilon_\rho \cdot \mathbf{p}, \quad (7)$$

where j_{em}^μ is the electromagnetic current and $H_{sb}(0)$ is the Hamiltonian density responsible for meson decay. We see that here f_ρ is simply a constant (independent of p) even when the ρ has internal structure and that the strong decay involves only the single form factor g_1 [compare to Eq. (2)]. The full Feynman amplitude, in contrast, would in general involve g_2 and an f_ρ dependent on $p = (\frac{1}{4}s - m_\pi^2)^{1/2}$. Moreover, the two matrix elements (6) and (7) can be readily computed in various models. The electromagnetic decay constant f_ρ in the quark model involves only $\psi_\rho(0)$, where $\psi_\rho(r)$ is the spatial wave function of the created $q\bar{q}$ pair in the ρ meson. The form factor g_1 can, for example, be computed in the flux-tube breaking (see Ref. 17) or quark-pair creation (see Ref. 18) model. Thus, the physics, and therefore the mass dependence, of the non- Z diagrams for $e^+e^- \rightarrow \rho \rightarrow \pi^+\pi^-$ is, while model dependent, relatively straightforward. An analogous situation holds for the more complicated process $\tau \rightarrow \nu_\tau \pi\pi\pi$.

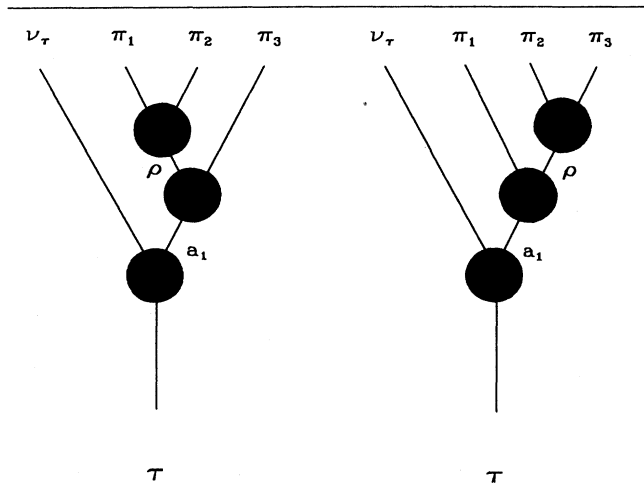


FIG. 2. Some covariant graphs contributing to $\tau \rightarrow \nu_\tau \pi_1 \pi_2 \pi_3$ via the a_1 and ρ intermediate states. The blobs represent general vertex functions.

C. The rate for $\tau \rightarrow \nu_\tau \pi \pi \pi$

With these observations in mind, it would be natural to calculate $\tau \rightarrow \nu_\tau \pi \pi \pi$ via the non- Z graphs corresponding to sequential processes such as $\tau \rightarrow \nu_\tau a_1$, $a_1 \rightarrow \rho \pi$, $\rho \rightarrow \pi \pi$, and $\tau \rightarrow \nu_\tau \pi'$, $\pi' \rightarrow \rho \pi$, $\rho \rightarrow \pi \pi$. For several reasons, one of which is the desire to represent the effects of Z graphs, one would then add to these resonant graphs a parametrized nonresonant amplitude.

Given that the nonresonant background amplitude is unknown, it is much more convenient computationally (as opposed to conceptually) to proceed by another route. We restore covariance to the amplitude, but we do so taking care that (1) the resonant portion of the amplitude is exactly the time-ordered one analogous to the one we have analyzed and understood above and (2) the parametrization of the nonresonant background amplitude is sufficiently rich that it can cancel the spurious effects of the Z graphs induced by making the resonant amplitude part of a covariant amplitude.

There is no unique implementation of this procedure, as one might suspect from, e.g., the fact that Eq. (1) has five amplitudes while the on-shell vertex has only two. However, it is obviously convenient to choose an implementation which, in some sense, keeps unwanted Z graphs associated with the resonant graph to a minimum. One might, ¹³⁻¹⁶ for instance, take $f_3 = f_4 = f_5 = 0$ in Eq. (1). While certainly an acceptable alternative, this choice produces a vertex $\Gamma^{\mu\nu}(a_1 \rightarrow \rho \pi)$ which can annihilate pseudoscalar components of an off-shell a_1 and create scalar components in an off-shell ρ . This means that the nonresonant parts of the covariant amplitudes would appear even in channels with the “wrong” quantum numbers with respect to our resonant time-ordered amplitude. We therefore choose the route of constraining the vertex factors $\Gamma^{\mu\nu}(a_1 \rightarrow \rho \pi)$ and $\Gamma^\mu(\rho \rightarrow \pi_1 \pi_2)$ so that they may produce only transversely polarized vector particles *even off shell* by demanding $p_\rho^\mu \Gamma_\mu = p_{a_1}^\mu \Gamma_{\mu\nu} = p_\rho^\nu \Gamma_{\mu\nu} = 0$. This choice has the additional advantage that its vertices annihilate the $k^\mu k^\nu$ part of the vector propagators which are relatively complicated for broad, off-shell particles. The results of applying these constraints to the vertices we need are presented in Appendix A, as are the full vector propagators and a brief derivation of the $\tau \rightarrow \nu_\tau \pi \pi \pi$ rate. A quark-model calculation of all necessary couplings is described in Appendix B.

III. RESULTS

As the discussion of Sec. II emphasizes, we must allow, in addition to the a_1 and π' resonances expected in this region, a general nonresonant background amplitude. However, an initial fit to the data without such background indicates that the resonant terms are dominant. As a result we need not be very sophisticated in our parametrization of the background amplitude—any scheme that can represent small, smooth effects will suffice. We proceed on two fronts.

(1) We modify the suspect Z -graph terms present in the covariant (but now by choice transverse) a_1 amplitude. Given the quality of the initial resonant fit, we are

satisfied to do this by considering simple modifications to the covariant a_1 propagator. Our procedure is to decompose

$$P(s) \equiv [s - m_{a_1}^2(s) + im_{a_1} \Gamma_{a_1}(s)]^{-1} \\ = P_{\text{res}}(s) + P_{\text{nonres}}(s), \quad (8)$$

where $m_{a_1}(s)$ is the covariant running mass of Eq. (A8), m_{a_1} is the a_1 on-resonance mass defined below Eq. (A8), and

$$P_{\text{res}}(s) = \{2m_{a_1}[\sqrt{s} - \bar{m}_{a_1}(s)] + im_{a_1} \Gamma_{a_1}(s)\}^{-1} \quad (9)$$

is the purely resonant time-ordered piece of the propagator $P(s)$ in the rest frame of the a_1 , with $\bar{m}_{a_1}(s)$ the mass function due to coupling with only those states involved in the resonant propagator (see Appendix A). We then study the effect on the deduced a_1 parameters from the replacement

$$P(s) \rightarrow P(s; \alpha) \equiv P_{\text{res}}(s) + \alpha P_{\text{nonres}}(s) \quad (10)$$

in the rate formula (A10) of Appendix A, with $0 \leq \alpha \leq 1$.

(2) We add an incoherent polynomial background rate term defined by

$$\frac{d\Gamma_b}{ds} = \frac{(m_\tau^2 - s)^2}{s} \sum_{n=1}^3 c_n (s - 9m_\pi^2)^n, \quad (11)$$

where the c_n 's are fitting parameters. Such a term allows us to take into account many possible small effects, including transverse Z -graph effects that cannot be described simply by $\alpha \neq 1$, nontransverse Z -graph effects, contributions from other channels (e.g., the low-mass tails of radial excitations of the a_1 and ρ and the high-mass tail of the pion) and residual experimental backgrounds.

With some prejudices based on the discussions in Sec. II, various fits to the data led us to define a “preferred fit” shown in Fig. 3 with the following ingredients.

(1) An a_1 with properties as described in the Appendices but with $\alpha = 0$ in its propagator [see Eq. (10)] and with the mass shift given in (A31) ignored. The choice $\alpha = 0$ is suggested but not required by the fits (see below); we prefer it since Z -graph suppression is expected on the grounds discussed above. (It should be noted that $\alpha = 0$ corresponds to Z -graph suppression in the a_1 rest frame and cannot strictly be interpreted as effecting such a suppression in general.) The decision to neglect the s dependence of the mass shift arises from our inability to calculate it with confidence; see the discussion in Sec. IV. We also ignore the mass shift in the ρ -meson propagator.

(2) A π' with the properties predicted in the Appendices. The addition of a π' is not required by our fits, but we include it in our “preferred fit” because it is unequivocally expected with properties we are convinced cannot be too far from those we use. The total width appearing in the π' propagator contains, in addition to the partial width for $\pi' \rightarrow (\pi\pi)_\rho \pi$, a constant allowing for the decay $\pi' \rightarrow (\pi\pi)_S \pi$ via the broad $\pi\pi S$ wave; the value of this constant is taken to be 150 MeV.

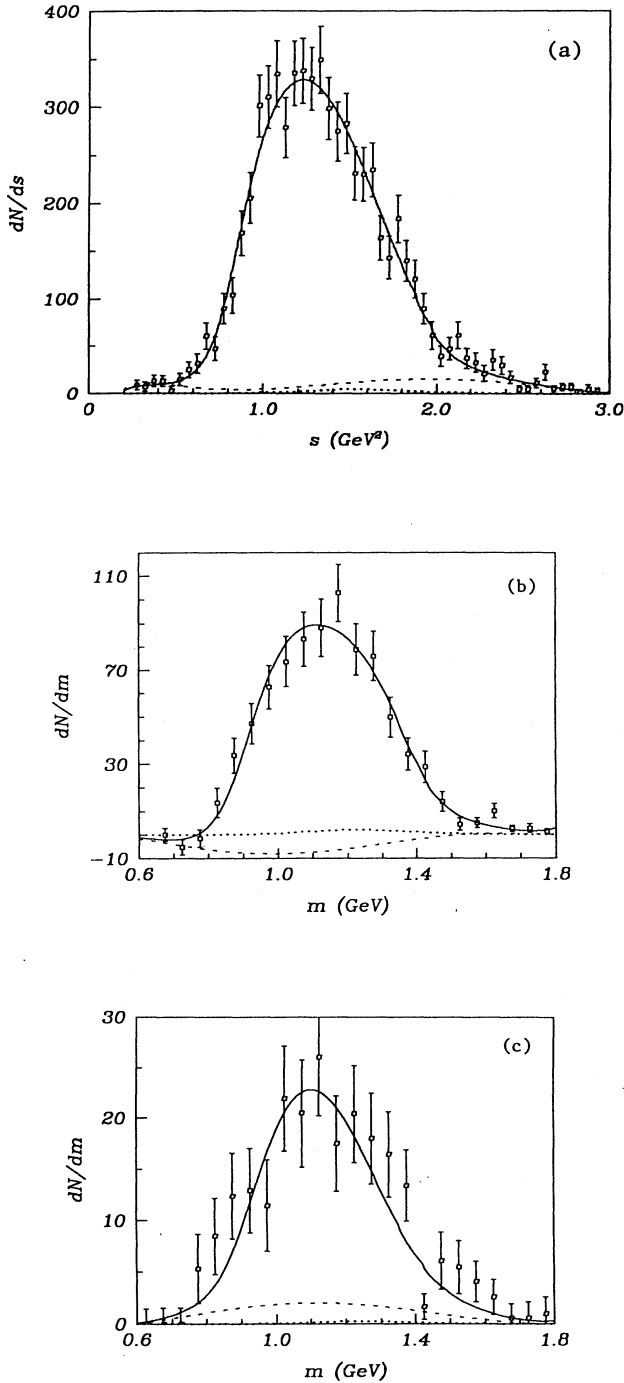


FIG. 3. Fits to experimental three-pion mass spectra (Refs. 2–4) from $\tau \rightarrow \nu_\tau \pi \pi \pi$. The solid curves are the “preferred fits” described in the text. The dashed curves show the fitted background polynomials of Eq. (11) and the dotted curves the predicted effect of the π' . The theoretical curves have been convoluted with a detector resolution function via Eq. (A32) with A , B as indicated: (a) ARGUS (Ref. 4); $A=0.0$ GeV, $B=0.030$; (b) Mark II (Ref. 3); $A=0.0$ GeV, $B=0.065$; (c) DELCO (Ref. 2); $A=0.0$ GeV, $B=0.065$. The values of A and B for the DELCO results are taken from Ref. 2; those for ARGUS and Mark II were not available and are estimates.

(3) The polynomial background of Eq. (11) used to absorb various small residual effects described above which might otherwise distort the deduced a_1 properties.

While we prefer this fit, we use it mainly as the starting point for an exploration of uncertainties; i.e., we do not allow our preferences to have much influence on our conclusions about the ranges in which the true a_1 parameters lie. The delineation of these ranges is one of the main topics of the next section.

IV. DISCUSSION AND CONCLUSIONS

The discussion of the reliability of our results is not a simple matter since many of the uncertainties in our conclusions arise from theory, not experiment. An important ingredient of our analysis, as emphasized in Secs. II and III, is the isolation of the time-ordered resonant piece of the usual Feynman graph and our subsequent analysis of its off-mass-shell behavior. One consequence of this is that the weak decay constant f_{a_1} for the resonant part of the Feynman graph is expected to be approximately independent of $m_{3\pi}^2$ (see Appendix B for a discussion of possible deviations from constancy). Bowler’s analysis¹⁰ shows that this conclusion can be reached (within errors) on phenomenological grounds by fitting the data; our arguments provide a rationale for considering the mass dependence of f_{a_1} to be known and hence reduce this source of error on the fitted a_1 mass and width.

However, a significant number of other uncertainties remain. The situation is summarized in Table II where we show the results and qualities of various fits.

(1) “Preferred”: This is the fit described above. It always gives acceptable confidence levels and no other fits we try ever provide any significant improvements.

(2) $\alpha \rightarrow 1$: This fit explores the importance of the suppression of Z graphs due to setting $\alpha=0$ in the preferred fit [see Eq. (10)]. We note that χ^2 is a very flat function of α . (The $\alpha=0$ value is preferred by the ARGUS data by about one standard deviation.) The fitted a_1 parameters are, however, insensitive to this change, the effect being absorbed into the background constants c_n of Eq. (11).

(3) $m_{a_1} \rightarrow \bar{m}_{a_1}(s)$: This fit includes the mass function $\bar{m}_{a_1}(s)$ appearing in the resonant a_1 propagator of Eq. (9). We consider our computed $\bar{m}_{a_1}(s)$ to be considerably less reliable than, e.g., our $\Gamma_{a_1}(s)$ [see point (7) below]. This is simply because such a mass function depends on the coupling of the resonance to all other channels, whereas our formulas include only the coupling to $\rho\pi$ and $K^*\bar{K} + \bar{K}^*K$. When only the $\rho\pi$ channel is considered, this mass function increases rather dramatically through the resonance. The coupling to $K^*\bar{K} + \bar{K}^*K$ considerably lessens this effect and we expect higher channels to further flatten this function near the a_1 resonance. These uncertainties lead us to exclude this effect from our “preferred” fit, but as fit 3 shows, the data alone cannot exclude the possibility that such effects are important. [Note that for simplicity we have ignored SU(3)-symmetry-breaking effects on the relative strength of the

TABLE II. Various fits to the ARGUS (Ref. 4), Mark II (Ref. 3), and DELCO (Ref. 2) three-pion mass spectra. “Preferred” refers to the fit described in Sec. III. Each of the subsequent fits differs from fit 1 only by the change indicated in the first column. “Best estimate” values are based on the distinct fits 1, 2, 3, 4, and 7 weighted by both the statistical confidence levels (C.L.) of the fits and to some extent our confidence in the physics of the fits. The numbers quoted are therefore somewhat subjective.

Fit	ARGUS			Mark II			DELCO		
	m_{a_1} (GeV)	Γ_{a_1} (GeV)	C.L.	m_{a_1} (GeV)	Γ_{a_1} (GeV)	C.L.	m_{a_1} (GeV)	Γ_{a_1} (GeV)	C.L.
(1) “Preferred”	1.213±.011	0.434±.030	0.54	1.25±.05	0.58±.10	0.51	1.18±.06	0.43±.19	0.12
(2) $\alpha \rightarrow 1$	1.219±.010	0.396±.024	0.37	1.24±.03	0.49±.07	0.56	1.19±.06	0.42±.15	0.14
(3) $m_{a_1} \rightarrow \bar{m}_{a_1}(s)$	1.236±.012	0.349±.019	0.36	1.26±.04	0.41±.05	0.36	1.22±.07	0.37±.12	0.16
(4) $c_n \rightarrow 0$	1.242±.011	0.487±.025	0.04	1.25±.02	0.51±.06	0.24	1.22±.04	0.57±.13	0.18
(5) $f_{\pi'} \rightarrow 0$	1.215±.011	0.434±.029	0.54	1.25±.04	0.57±.09	0.50	1.18±.06	0.43±.18	0.12
(6) $f_{a_1 \rho \pi}^D \rightarrow 0$	1.212±.011	0.436±.029	0.56	1.25±.04	0.58±.10	0.48	1.18±.06	0.43±.19	0.11
(7) $\beta \rightarrow 0.3$ GeV	1.203±.008	0.376±.022	0.15	1.22±.02	0.47±.06	0.63	1.19±.05	0.48±.14	0.18
(8) No $K^* \bar{K} + \bar{K}^* K$	1.207±.009	0.421±.026	0.53	1.21±.03	0.49±.08	0.27	1.17±.05	0.37±.17	0.10
Best estimate	1.220±.015	0.400±.045		1.24±.04	0.49±.09		1.20±.06	0.46±.16	

$K^* \bar{K}$ and $\rho\pi$ couplings.] Our inability to reliably predict $\bar{m}_{a_1}(s)$ represents, in our opinion, the greatest source of uncertainty in extracting the a_1 mass and width from the data.

The importance of the mass function $m_{a_1}(s)$ (and the $K^* \bar{K} + \bar{K}^* K$ channel) has also been considered recently by Törnqvist (see Ref. 19). He found that the inclusion of these two effects markedly *increases* both the fitted a_1 mass and width. [Note that in Table I of that reference, the values in parentheses correspond to the “usual” Breit-Wigner in which $m_{a_1}(s)$ is taken to be constant and the $K^* \bar{K} + \bar{K}^* K$ channel is neglected.] However, we find that the fitted a_1 width would *decrease* on including the running mass and the $K^* \bar{K} + \bar{K}^* K$ channel. This discrepancy arises mainly from our use of hadronic form factors rather than the pointlike couplings employed in Ref. 19. The form factors generate a mass-dependent a_1 width which falls off at high mass in contrast with the indefinitely increasing width of Ref. 19. The effect of including a running mass which rises through the resonance is to increase the fitted resonance mass and decrease the width, whereas the result of introducing the $K^* \bar{K} + \bar{K}^* K$ channel in the total mass-dependent width is an increase in both the a_1 mass and width. Thus, considering both the running mass and the $K^* \bar{K} + \bar{K}^* K$ channel increases the fitted value of the mass regardless of the choice of couplings. The effect on the width, in contrast, is not model independent: for pointlike couplings, the effect of the large width at high mass dominates and leads to an increased width on resonance as found by Törnqvist, while in our model the width would decrease slightly.

(4) $c_n = 0$: Here we see that some sort of nonresonant amplitude is required by the data as the confidence level of the fit with the c_n of Eq. (11) set to zero drops dramatically. This is to be expected, but fortunately the a_1 parameters do not shift very much despite this large decrease in the quality of the fit. Note that the main effect of the c_n terms is to reduce the sensitivity of our conclusions to the tails of the distributions.

(5) $f_{\pi'} = 0$: The absence of the radial excitation of the pion with the properties predicted in Appendix B has essentially no effect on our conclusions concerning the parameters of the a_1 . However, if we were to allow a large $\pi'(1300)$ contribution, our conclusions might be affected. This possibility could be ruled out experimentally by studying the 3π Dalitz plot.

(6) $f_{a_1 \rho \pi}^D = 0$: Our model predicts the ratio of the D - and S -wave amplitudes in $a_1 \rightarrow (\pi\pi)_\rho \pi$ to be $A[a_1 \rightarrow (\rho\pi)_D] / A[a_1 \rightarrow (\rho\pi)_S] = -0.15$. Since the addition of the predicted D wave produces theoretical $\pi\pi$ projections of the 3π Dalitz plot in better agreement with experiment, as indicated in Fig. 4, we have little reason to worry that this model dependence is adversely affecting our conclusions. We also have the known success of the model for the analogous D/S ratio in $b_1 \rightarrow \omega\pi$ to support our confidence. This fit shows that our conclusions on the a_1 mass and width are in any event insensitive to this ratio. The value of D/S extracted from a fit to the experimental Dalitz-plot projections is given in Table III and agrees well with our model’s prediction.

(7) $\beta \rightarrow 0.3$ GeV: The mass dependence of the hadronic form factors derived in Appendix B is already well tested by studies of strong decay processes. For example, the $\pi\pi$ partial widths of the natural-parity sequence $\rho(770)$, $f_2(1270)$, $\rho_3(1690)$, $f_4(2030)$, . . . , are well described by our model even though they contain relative phase-space factors $(p/p_0)^{2L+1}$ which are very sensitive to the intrinsic scale p_0 of the transition.¹⁷ Also, the model actually predicts with surprising accuracy the absolute width of the a_1 . There are, nevertheless, reasons to be skeptical—the apparently similar electromagnetic form factors computed with the same wave functions are too hard; i.e., they drop too slowly with q^2 . We have accordingly considered the effects of varying the form-factor slope parameter β (see Appendix B) from 0.4 GeV to 0.3 GeV in this fit. The χ^2 change indicates that, as in the global fit, smaller β values are not preferred.

(8) No $K^* \bar{K} + \bar{K}^* K$: Not only does the $K^* \bar{K} + \bar{K}^* K$ channel have a dramatic effect on the mass shift function, but also, as this fit shows, its inclusion in the total mass-

dependent a_1 width has an effect on the deduced resonance parameters.

On considering the uncertainties discussed here and in Sec. III, we are led to the conclusions listed in Table III. In addition to noting the consistency of our mass and width (see Ref. 20) for the a_1 with the standard values⁹ based on hadronic reactions,^{6,7} we would like to make a few comments on some of the implications of these and

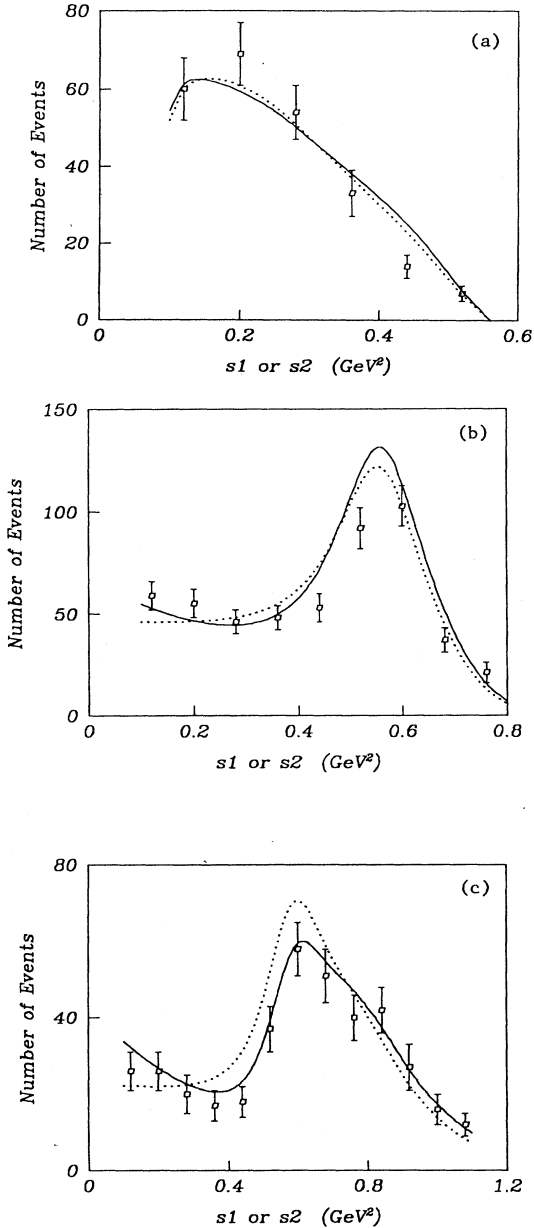


FIG. 4. Comparison to experimental (Ref. 4) two-pion mass projections of the three-pion Dalitz plot for various three-pion-mass bins. The solid curves correspond to the “preferred fit” described in the text and the dotted curves to the fit with the $a_1 \rightarrow \rho\pi$ D -wave amplitude arbitrarily set to zero (fit 6 of Table II). (a) $0.81 \text{ GeV}^2 \leq m_{3\pi}^2 \leq 1.1025 \text{ GeV}^2$, (b) $1.1025 \text{ GeV}^2 \leq m_{3\pi}^2 \leq 1.44 \text{ GeV}^2$, (c) $1.44 \text{ GeV}^2 \leq m_{3\pi}^2 \leq 1.96 \text{ GeV}^2$.

TABLE III. Parameters extracted from $\tau \rightarrow \nu_\tau \pi \pi \pi$. The quoted mass and width come from a weighted average of the values in the last row of Table II. The value of f_{a_1} is derived from the absolute rate for $\tau \rightarrow \nu_\tau \pi \pi \pi$. The D/S ratio is extracted from fits to the Dalitz-plot projections of Fig. 4.

m_{a_1} (MeV)	1220 ± 15
Γ_{a_1} (MeV)	420 ± 40
f_{a_1} (GeV^2)	0.25 ± 0.02
D/S	-0.14 ± 0.03
$m_{\pi'}$	No significant constraint
$\Gamma_{\pi'}$	No significant constraint

the other parameters of Table III. Our comments are very incomplete: we focus mainly on interpreting the results listed there within the constituent-quark model.

We begin with the mass. In the quark model it is sensitive to an interplay of spin-orbit and hyperfine interactions. A mass in the range we have extracted points to a nonzero contact interaction in the P -wave mesons as expected in relativistic quark models (see, e.g., Ref. 21). This is because

$$\frac{1}{9}(5m_{a_2} + 3m_{a_1} + m_{a_0}) - m_{b_1} = 32 \pm 19 \text{ MeV} \quad (12)$$

would be zero with only spin-orbit and tensor interactions. [We have used $m_{a_0} = 1.15 \pm 0.15 \text{ GeV}$ in this relation since although the $^3P_0 a_0$ probably cannot be associated with the $a_0(980)$, it is still expected in the 1.0–1.3-GeV mass range.] Its sign is as expected (the same as the ρ - π splitting), as is its magnitude.

In addition to the nonzero combination of masses given in (12), the observation that $f_{a_1} \neq 0$ also reveals the failure of the “wave function at the origin” approximation. Since the weak current creates the $u\bar{d}$ pair in the a_1 at a point, f_{a_1} is also proportional to $\psi(0)$ and vanishes in the $L=1$ states in the nonrelativistic limit. It has been appreciated for some time that nonleading terms in \mathbf{p}/m give a substantial value to the a_1 weak decay constant (see Ref. 22). The value we extract in Table III is consistent with such expectations (see Appendix B). It is also roughly consistent with expectations from current-algebra sum rules (see Ref. 23).

The a_1 width of Table III and the D/S ratio provide rather stringent tests of models of hadronic decay. In the context of the quark model they provide important tests of the connection between the spin-singlet decay $b_1 \rightarrow \omega\pi$ and the spin-triplet decays such as $a_1 \rightarrow \rho\pi$. Indeed, both the simplistic elementary-pion-emission model (see Ref. 21) and the flux-tube-breaking model^{17,18} give

$$A(a_1 \rightarrow (\rho\pi)_S) = \sqrt{32} S_1, \quad (13)$$

$$A(b_1 \rightarrow (\omega\pi)_S) = -\sqrt{8} S_1, \quad (14)$$

$$A(a_1 \rightarrow (\rho\pi)_D) = -D_1, \quad (15)$$

$$A(b_1 \rightarrow (\omega\pi)_D) = -D_1, \quad (16)$$

where S_1 and D_1 are (in general, momentum-dependent)

S - and D -wave amplitudes. The flux-tube-breaking model predicts D_1/S_1 independent of any free parameters, while in the elementary pion emission model this ratio is determined by fits to other decays. Both models give the observed D/S ratio in $b_1 \rightarrow \omega\pi$ and are consistent with both the D/S ratio in $a_1 \rightarrow \rho\pi$ extracted here as well as the total $a_1 \rightarrow \rho\pi$ decay rate. In addition to the importance of this result in its own right, it lends further credence to the observation¹ based on these models that the S -wave decays of the known scalar mesons $f_0(975)$ and $a_0(980)$ are inconsistent with those of the 3P_0 quark-model partners of the a_2 , a_1 , and b_1 .

It is unfortunate that $\tau \rightarrow \nu_\tau \pi \pi \pi$ provides no evidence at this time for the radially excited pion. The observation of the π' , or its nonobservation at the level expected, has important implications in the search for pseudoscalar glueballs. The radially excited isoscalar pseudoscalars should be produced in $\gamma\gamma$ collisions by a mechanism similar to that which makes the π' in τ decay. The present lack of evidence for these states is hampering the study of possible glueballs with $J^{PC}=0^{-+}$; information on the π' could be the key to understanding this whole sector. It is possible that such considerations alone would justify a higher-statistics study of the $\tau \rightarrow \nu_\tau \pi \pi \pi$ Dalitz plot for pseudoscalar contributions. The experimental determination of the $J^{PC}=0^{-+}$ background in this Dalitz plot would also allow a more accurate determination of the a_1 parameters.

A higher-statistics study of $\tau \rightarrow \nu_\tau \pi \pi \pi$ could improve our understanding of the a_1 in other ways. It would, first of all, directly reduce the errors in the a_1 parameters, although with a reduction in experimental errors by a factor of 2 these would become dominated by theoretical uncertainties. The availability of meaningful data at higher- 3π mass would indirectly reduce theoretical uncertainties by providing a measurement of backgrounds (both axial-vector and pseudoscalar) off resonance which could be extrapolated under the resonance. Very-high-quality data might also see or limit the effect of the opening of the $K^* \bar{K} + \bar{K}^* K$ channel for a_1 decay, thereby eliminating a further theoretical uncertainty. There are also, unquestionably, improvements that can be made in our theoretical understanding of these decays including careful study of the presumed small residual mass dependence of f_{a_1} , direct calculation of the Z -graph suppressions, consideration of higher mass virtual channels, the study of theoretical and phenomenological constraints on the momentum dependence of strong form factors, etc. We believe that such experimental and theoretical efforts are well justified and could lead to a substantial improvement in our knowledge of the a_1 and π' . However, we must also acknowledge that the large width of the a_1 presents a barrier to a precise determination of its properties that, at least for now, remains.

ACKNOWLEDGMENTS

We gratefully acknowledge the hospitality of the Department of Theoretical Physics and the Department of Nuclear Physics, Oxford, where this work was com-

pleted. We are particularly indebted to M. G. Bowler for conversations. This work was supported in part by a grant from the Natural Sciences and Engineering Research Council of Canada.

APPENDIX A: VERTICES, PROPAGATORS, AND THE DIFFERENTIAL DECAY RATE

To construct the covariant amplitude corresponding to Fig. 2 (and the analogous π' graphs) one needs the appropriate vertices and propagators. As discussed in the text we choose our vertices to be transverse. Thus, with the labeling of Fig. 5 and with the pions all on-mass shell, the vertex factors may be written

$$\Gamma^{\mu\nu}(a_1 \rightarrow \rho\pi) = f_{a\rho\pi}(q^2, k^2) \left[-g^{\mu\nu} + \frac{k^\mu k^\nu}{k^2} + \frac{q^\mu q^\nu}{q^2} - \frac{k \cdot q}{k^2 q^2} q^\mu k^\nu \right] + g_{a\rho\pi}(q^2, k^2) \left[\frac{k \cdot q}{q^2} q^\mu - k^\mu \right] \left[q^\nu - \frac{k \cdot q}{k^2} k^\nu \right], \quad (\text{A1})$$

$$\Gamma^\nu(\rho \rightarrow \pi_2 \pi_3) = -i f_{\rho\pi\pi}(k^2) (p_2^\nu - p_3^\nu), \quad (\text{A2})$$

$$\Gamma^\nu(\pi' \rightarrow \rho\pi) = i f_{\pi'\rho\pi}(q^2, k^2) \left[q^\nu - \frac{k \cdot q}{k^2} k^\nu \right], \quad (\text{A3})$$

where the form factors are all real. They are calculated in Appendix B in the flux-tube-breaking model.

The propagator $G^{\mu\nu}(k)$ of the interacting a_1 or ρ is given by the self-energy diagrams of Fig. 6. With the "bare" propagator $G_0^{\mu\nu}$ given by

$$-iG_0^{\mu\nu}(k) = \frac{-g^{\mu\nu} + k^\mu k^\nu / m_0^2}{k^2 - m_0^2 + i\epsilon}, \quad (\text{A4})$$

where m_0 is the "bare" mass, and the one-particle-irreducible bubble $\omega_{\mu\nu}$ of the general form

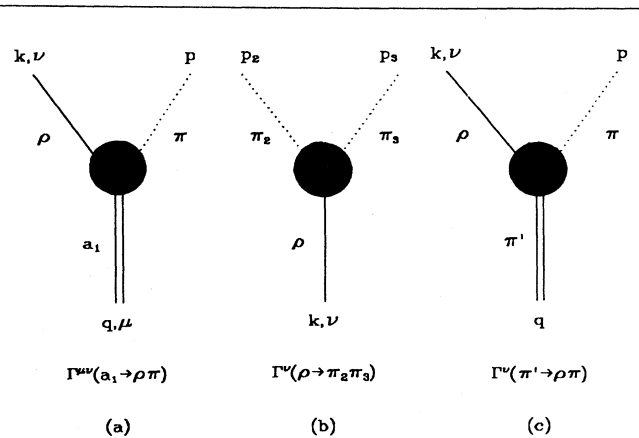


FIG. 5. (a) The $a_1 \rightarrow \rho\pi$ vertex, (b) the $\rho \rightarrow \pi_2 \pi_3$ vertex, (c) the $\pi' \rightarrow \rho\pi$ vertex; in all cases the momentum flow of the lines is from the bottom to the top of the diagram so $q = k + p$ and $k = p_2 + p_3$.

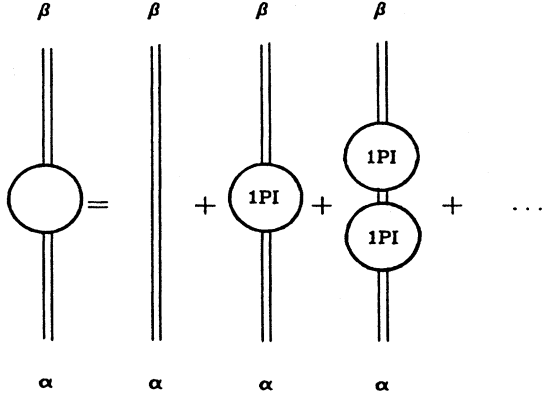


FIG. 6. The propagator $G^{\beta\alpha}(k) = G_0^{\beta\alpha}(k) + G_0^{\beta\nu}(k)\omega_{\nu\mu}(k)G_0^{\mu\alpha} + \dots$ as a sum over one-particle-irreducible (1PI) bubbles.

$$\omega_{\mu\nu}(k) = -i[\omega_1(k^2)(-g_{\mu\nu} + k_\mu k_\nu/k^2) - \omega_2(k^2)k_\mu k_\nu/k^2], \quad (\text{A5})$$

one finds, since $G^{-1} = G_0^{-1} - \omega$, that

$$-iG_{\mu\nu}(k) = \frac{-g_{\mu\nu} + \left[\frac{k^2 - \omega_1(k^2) + \omega_2(k^2)}{m_0^2 + \omega_2(k^2)} \right] k_\mu k_\nu/k^2}{k^2 - m_0^2 - \omega_1(k^2) + i\epsilon}. \quad (\text{A6})$$

With our use of transverse vertices, the $k^\mu k^\nu$ term conveniently never enters. For the π' , the full propagator is of course analogous, with the numerator in (A6) equal to unity. As usual we write

$$\omega_1(k^2) = m^2(k^2) - m_0^2 - im_R \Gamma_R(k^2), \quad (\text{A7})$$

so that the denominators are in the Breit-Wigner form

$$k^2 - m^2(k^2) + im_R \Gamma_R(k^2). \quad (\text{A8})$$

We define the mass m_R of the resonance to be the value of $m(k^2)$ when $m^2(k^2) = k^2$ and the on-resonance width to be $\Gamma_R(m_R^2)$.

If only the non- Z time-ordered graphs contained in Fig. 6 are summed, one obtains a noncovariant ‘‘resonant’’ propagator whose denominator is given by

$$2E_R \left[E - E_R - \delta E_R(E) + i \frac{\tilde{\Gamma}_R(E)}{2} \right], \quad (\text{A9})$$

where $E_R = \sqrt{\mathbf{k}^2 + m_R^2}$, $E = \sqrt{\mathbf{k}^2 + k^2}$, $\tilde{\Gamma}_R(E)$ is the mass-dependent width related to the covariant width by $\tilde{\Gamma}_R(E) = (m_R/E_R)\Gamma_R(k^2)$ and $\delta E_R(E)$ is the (renormalized) level shift satisfying $\delta E_R(E_R) = 0$.

With these factors in hand, it is straightforward to proceed to the rate. One finds by standard methods that

$$\frac{d^3\Gamma_{\tau \rightarrow \nu \tau^3 \pi}}{ds ds_1 ds_2} = \frac{G_F^2 \cos^2 \theta_C m_\tau^3}{16\pi^2 s} \left[1 - \frac{s}{m_\tau^2} \right]^2 \left[\left[1 + \frac{2s}{m_\tau^2} \right] \rho_a(s, s_1, s_2) + \rho_p(s, s_1, s_2) \right], \quad (\text{A10})$$

where ρ_a and ρ_p are axial-vector and pseudoscalar spectral densities, $s = (p_1 + p_2 + p_3)^2$, $s_1 = (p_2 + p_3)^2$, $s_2 = (p_1 + p_3)^2$, and $s_3 = (p_1 + p_2)^2$. For the a_1 resonance alone one has

$$\rho_a(s, s_1, s_2) = f_{a_1}^2 P_{a_1}(s) F_{a_1}(s_1, s_2), \quad (\text{A11})$$

while for the π' alone one has

$$\rho_p(s, s_1, s_2) = s f_{\pi'}^2 P_{\pi'}(s) F_{\pi'}(s_1, s_2), \quad (\text{A12})$$

where the f_n are the weak decay constants discussed in Appendix B (see Fig. 7), the covariant propagators are given by

$$P_n(s) = \{[s - m_n^2(s)]^2 + m_n^2 \Gamma_n^2(s)\}^{-1} \quad (\text{A13})$$

[note that for the a_1 propagator in our fits we use $P(s; \alpha)$ given in Eq. (10)] and

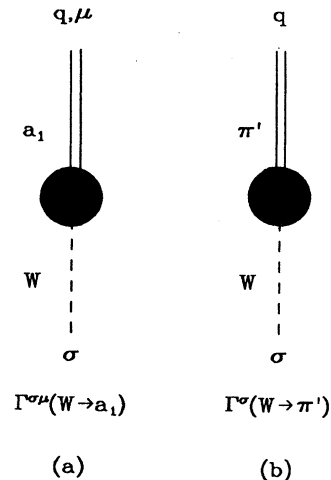


FIG. 7. (a) The $W \leftrightarrow a_1$ vertex and (b) the $W \leftrightarrow \pi'$ vertex.

$$F_n(s_1, s_2) = 2(8\pi)^{-3} [P_\rho(s_1)D_n(s_1, s_2) + P_\rho(s_2)D_n(s_2, s_1) + 2\Delta(s_1, s_2)I_n(s_1, s_2)], \quad (\text{A14})$$

in which

$$\Delta(s_1, s_2) = P_\rho(s_1)P_\rho(s_2) [(s_1 - m_\rho^2)(s_2 - m_\rho^2) + m_\rho^2 \Gamma_\rho(s_1)\Gamma_\rho(s_2)] \quad (\text{A15})$$

$$D_{a_1}(s_1, s_2) = [\tau_1^2(s_1, s_2)\mathbf{p}_1^2 + \tau_2^2(s_1, s_2)\mathbf{p}_2^2 + 2\tau_1(s_1, s_2)\tau_2(s_1, s_2)\mathbf{p}_1 \cdot \mathbf{p}_2] / 3s, \quad (\text{A17})$$

$$I_{a_1}(s_1, s_2) = \{\tau_1(s_1, s_2)\tau_2(s_2, s_1)\mathbf{p}_1^2 + \tau_1(s_2, s_1)\tau_2(s_1, s_2)\mathbf{p}_2^2 + [\tau_1(s_1, s_2)\tau_1(s_2, s_1) + \tau_2(s_1, s_2)\tau_2(s_2, s_1)]\mathbf{p}_1 \cdot \mathbf{p}_2\} / 3s, \quad (\text{A18})$$

while, for the radially excited pion,

$$D_\pi(s_1, s_2) = \tau_3^2(s_1, s_2) / s, \quad (\text{A19})$$

$$I_\pi(s_1, s_2) = \tau_3(s_1, s_2)\tau_3(s_2, s_1) / s, \quad (\text{A20})$$

where the functions appearing above are defined by

$$\tau_1(s_1, s_2) = f_{\rho\pi\pi}(s_1) [f_{a\rho\pi}(s, s_1) - \frac{1}{2}g_{a\rho\pi}(s, s_1)(s_3 - s_2)], \quad (\text{A21})$$

$$\tau_2(s_1, s_2) = 2f_{\rho\pi\pi}(s_1)f_{a\rho\pi}(s, s_1), \quad (\text{A22})$$

$$\tau_3(s_1, s_2) = \frac{1}{2}f_{\pi\rho\pi}(s, s_1)f_{\rho\pi\pi}(s_1)(s_3 - s_2), \quad (\text{A23})$$

and \mathbf{p}_1^2 , \mathbf{p}_2^2 and $\mathbf{p}_1 \cdot \mathbf{p}_2$ are expressed in terms of Lorentz invariants using

$$2\mathbf{p}_1 \cdot \mathbf{p}_2 = s_1 + s_2 - s - m_\pi^2 + 2E_1 E_2, \quad (\text{A24})$$

$$2\sqrt{s} E_i = s + m_\pi^2 - s_i, \quad (\text{A25})$$

$$\mathbf{p}_i^2 = E_i^2 - m_\pi^2. \quad (\text{A26})$$

The total mass-dependent widths appearing in (A13) are given by

and the width of the ρ meson is given by

$$\Gamma_\rho(s_i) = \Gamma_\rho(m_\rho^2) \left[\frac{m_\rho}{\sqrt{s_i}} \right] \left[\frac{f_{\rho\pi\pi}(s_i)}{f_{\rho\pi\pi}(m_\rho^2)} \right]^2 \left[\frac{s_i - 4m_\pi^2}{m_\rho^2 - 4m_\pi^2} \right]^{3/2}. \quad (\text{A16})$$

The direct (D) and interference (I) factors are most easily evaluated in the rest frame of n . For the a_1 we have

$$m_{a_1}\Gamma_{a_1}(s) = \int ds_1 ds_2 F_{a_1}(s_1, s_2) + m_{a_1}\Gamma_{a_1 K^* K}(s), \quad (\text{A27})$$

$$m_\pi\Gamma_\pi(s) = \int ds_1 ds_2 F_\pi(s_1, s_2), \quad (\text{A28})$$

with the width for the a_1 to decay to $K^* \bar{K} + \bar{K}^* K$ given by

$$m_{a_1}\Gamma_{a_1 K^* K}(s) = \frac{(\gamma^2 - \xi)^{1/2}}{24\pi\xi s} \left[f^2(2\xi + \gamma^2) + fg\gamma(\gamma^2 - \xi) + \frac{g^2}{4}(\xi - \gamma^2)^2 \right], \quad (\text{A29})$$

where $\xi = 4sm_{K^*}^2$, $\gamma = s - m_K^2 + m_{K^*}^2$, $f = f_{aK^* K}(s)$, and $g = g_{aK^* K}(s)$. We have restricted the sum over channels to $\rho\pi$ and $K^* \bar{K} + \bar{K}^* K$ for practical reasons. The mass shift functions are calculated from these widths using

$$m_n^2(s) = m_n^2 - \frac{1}{\pi} \mathbf{P} \int_{s_{\text{th}}}^{\infty} ds' \left[\frac{m_n\Gamma_n(s')}{s' - s} - \frac{m_n\Gamma_n(s')}{s' - m_n^2} \right], \quad (\text{A30})$$

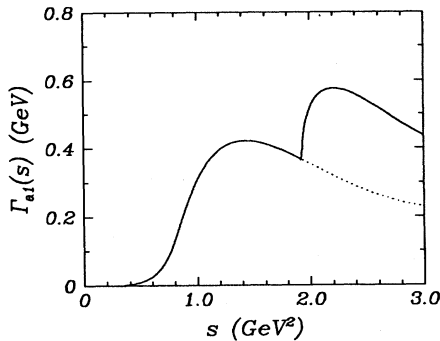


FIG. 8. The mass-dependent widths. The solid curve is the total mass-dependent a_1 width from Eq. (A27) including the $\rho\pi$ and $K^* \bar{K} + \bar{K}^* K$ channels assuming SU(3)-symmetric coupling relations. The dotted curve indicates the $a_1 \rightarrow (\pi\pi)_\rho\pi$ partial width.

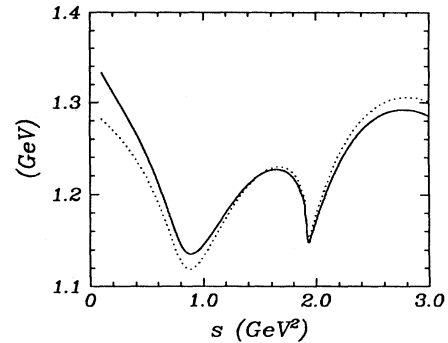


FIG. 9. The running mass functions. The dotted curve is the covariant mass function $m_{a_1}(s)$ from Eq. (A30); the solid curve shows the resonant running mass function $\bar{m}_{a_1}(s)$ given by Eq. (A31). Both the $\rho\pi$ and $K^* \bar{K} + \bar{K}^* K$ channels are included in these results.

$$\bar{m}_n(s) = m_n - \frac{1}{2\pi} \mathcal{P} \int_{m_{\text{th}}}^{\infty} dm' \left[\frac{\Gamma_n(m'^2)}{m' - \sqrt{s}} - \frac{\Gamma_n(m'^2)}{m' - m_n} \right]. \quad (\text{A31})$$

The width function of Eq. (A27) and these mass shift functions are shown in Figs. 8 and 9, respectively. Nu-

merical integrations over the Dalitz-plot variables s_1 and s_2 can be done at this stage either partially to produce projections corresponding to s_1 distributions as a function of s or fully to produce the three-pion-mass spectrum.

Finally, in order to compare our results with experiment, the theoretical results must be convoluted with a detector resolution function; e.g.,

$$\frac{d\Gamma_{\tau \rightarrow \nu_r 3\pi}^{\text{obs}}}{ds} = \frac{1}{m} \int_{-\infty}^{+\infty} dm' \frac{m'}{\sqrt{2\pi}\sigma(m')} \exp \left[-\frac{1}{2} \left(\frac{m-m'}{\sigma(m')} \right)^2 \right] \left[\frac{d\Gamma_{\tau \rightarrow \nu_r 3\pi}^{\text{ideal}}}{ds'} \right], \quad (\text{A32})$$

where $m = \sqrt{s}$, $m' = \sqrt{s'}$, and $\sigma(m') = A + Bm'$ with A and B constants.

APPENDIX B: FORM FACTORS

The extracted parameters of the a_1 can, in principle, depend on the mass dependence of the couplings which enter in (A1) and (A2) and in the weak vertex to be discussed below. They could also depend on the existence of important contributions to $\tau \rightarrow \nu_r \pi \pi \pi$ from other resonances. In this appendix we compute the form factors relevant to these issues in the quark model. The results provide a "base prediction" from which we explore the possible sensitivity of our results for the a_1 on such model-dependent effects.

We exploit the quark model by using the relativized mock-meson method (see Refs. 21 and 22). The basic idea of the method is that, in the weak-binding limit, the quark model provides a Lorentz-invariant decomposition of any matrix element which can be put in one-to-one correspondence with a physical matrix element of interest. One can therefore associate the true Lorentz-invariant form factors with quark-model formulas valid in the weak-binding limit. The mock-meson method then either uses these formulas or some relativized version of them with physical parameters. One thus assumes that the formulas, or some relativized version of them, can be extrapolated from the weak-binding limit ($\mathbf{p}^2/m^2 \ll 1$) to the physical case where in fact \mathbf{p}^2/m^2 is of order unity.

1. Weak vertices

The a_1 and π' weak vertices corresponding to Fig. 7 are (see Ref. 24)

$$\Gamma^{\sigma\mu}(W \rightarrow a_1) = -if_{a_1}(q^2)g^{\sigma\mu}, \quad (\text{B1})$$

$$\Gamma^{\sigma}(W \rightarrow \pi') = -f_{\pi'}(q^2)q^{\sigma}. \quad (\text{B2})$$

In general, the q^2 dependence of these weak form factors is unknown. However, as explained in the text we wish to use the q^2 dependence appropriate to the time-ordered resonant graphs. In the approximation where only the direct $W \rightarrow a_1$ and $W \rightarrow \pi'$ processes contribute, this dependence is trivial since the time-ordered graphs just involve the off-energy-shell but otherwise physical inter-

mediate states and hence the on-mass-shell matrix elements

$$\langle a_1(\mathbf{p}_a, s_a) | A^{\dagger\mu}(0) | 0 \rangle = f_{a_1} \epsilon^{*\mu}(\mathbf{p}_a, s_a) \quad (\text{B3})$$

[analogous to Eq. (6)] and

$$\langle \pi'(\mathbf{p}_{\pi'}) | A^{\dagger\mu}(0) | 0 \rangle = -if_{\pi'} p_{\pi'}^{\mu}, \quad (\text{B4})$$

where f_{a_1} and $f_{\pi'}$ are constants and $A^{\mu}(0)$ is the axial-vector current. There are, it should be noted, higher-order graphs which can give energy dependence to these form factors. If, for example, we relax the assumption that the a_1 is excited directly by the W but still maintain the assumption of resonance dominance (which should be reliable), then the a_1 could be excited indirectly via the process $W \rightarrow a_1' \rightarrow a_1$. Here, the a_1' is a radial excitation of the a_1 and the $a_1' \leftrightarrow a_1$ mixing can occur via common strong (virtual or real) decay channels. Since such a mixing is unlikely to be strong and given that it would in the first approximation be energy independent, it should be safe to ignore corrections to the $f_{a_1} = \text{const}$ approximation.

The weak decay constants appearing in (B3) and (B4) can be estimated in the mock-meson method which gives

$$f_{a_1} = \frac{4\sqrt{2\pi} \bar{M} a_1^{1/2}}{(2\pi)^{3/2}} \int_0^{\infty} dp p^2 R_{a_1}(p) \left[\frac{p}{E} \right] \left[\frac{m}{E} \right]^{\epsilon_1}, \quad (\text{B5})$$

$$f_{\pi'} = \frac{-4\sqrt{3\pi}}{(2\pi)^{3/2} \bar{M} \pi'^{1/2}} \int_0^{\infty} dp p^2 R_{\pi'}(p) \left[\frac{m}{E} \right]^{1+\epsilon_2}, \quad (\text{B6})$$

where $\phi_{nlm}(\mathbf{p}) \equiv (-i)^l R_{nl}(p) Y_{lm}(\Omega_p)$ is the unit normalized momentum-space wave function, m is the constituent quark mass, and $E = (\mathbf{p}^2 + m^2)^{1/2}$. We determine the wave functions by diagonalizing the nonrelativistic Coulomb-plus-linear-potential problem

$$V(r) = -\frac{4\alpha_s}{3r} + br + c \quad (\text{B7})$$

in a harmonic-oscillator basis with the harmonic-oscillator parameter used as a variational parameter. The constants of the potential are $c = -0.84$ GeV, $\alpha_s = 0.5$, and $b = 0.18$ GeV²; the quark mass is 0.33 GeV and the mock-meson masses \bar{M} are both taken to be 1.3 GeV. The factors of $(m/E)^{\epsilon_i}$ in (B5) and (B6) are inserted to al-

TABLE IV. The weak decay constants. f_{a_1} and f_{π^*} are calculated using (B5) and (B6); f_{π} is determined using an equation analogous to (B6). The parameters ϵ_i are those in Eqs. (B5) and (B6). The experimental value quoted for f_{a_1} is determined from a fit to the absolute rate for $\tau \rightarrow \nu_{\tau} \pi \pi \pi$.

	$\epsilon_i=0$	$\epsilon_i=\frac{1}{2}$	$\epsilon_i=1$	Experimental value
f_{π} (GeV)	0.19	0.14	0.11	0.132
f_{a_1} (GeV ²)	0.22	0.16	0.12	0.25±0.02
f_{π^*} (GeV)	0.08	0.04	0.02	

low for relativistic corrections, as suggested in Ref. 21. Table IV shows the results obtained from (B5), (B6), and the analogous formula for f_{π} as a function of the parameter ϵ_i . Since relativistic corrections are expected to be more important in the pion than in the a_1 , it is not surprising that the pion favors a larger value for ϵ_i . For the fits of the text we take $f_{\pi^*}/f_{a_1}=0.2 \text{ GeV}^{-1}$.

2. Strong vertices

The strong form factors $f_{a\rho\pi}$, $g_{a\rho\pi}$, and $f_{\rho\pi\pi}$ defined in Appendix A can be computed by similar methods. Since they involve the creation of an additional $q\bar{q}$ pair, they are less trivial dynamically than the weak form factors which just involve the action of a current. As previously mentioned, we compute them in the flux-tube-breaking model¹⁷ in the 3P_0 limit.¹⁸ Since, once again, we wish to build in the mass dependence appropriate to the time-ordered resonant graphs, we study (A1)–(A3) for physical states, where we have

$$\langle \rho(p_{\rho} s_{\rho}) \pi(p_{\pi}) | H_{sb}(0) | a_1(p_a s_a) \rangle = -i \epsilon_{\nu}^*(p_{\rho} s_{\rho}) (f_{a\rho\pi} g^{\nu\mu} + g_{a\rho\pi} p_a^{\nu} p_{\rho}^{\mu}) \epsilon_{\mu}(p_a s_a), \quad (\text{B8})$$

$$\langle \rho(p_{\rho} s_{\rho}) \pi(p_{\pi}) | H_{sb}(0) | \pi'(p_{\pi'}) \rangle = -f_{\pi'\rho\pi} \epsilon_{\mu}^*(p_{\rho} s_{\rho}) p_{\pi'}^{\mu}, \quad (\text{B9})$$

$$\langle \pi(p_1) \pi(p_2) | H_{sb}(0) | \rho(p_{\rho} s_{\rho}) \rangle = f_{\rho\pi\pi} \epsilon_{\mu}(p_{\rho} s_{\rho}) (p_1 - p_2)^{\mu}. \quad (\text{B10})$$

$$\langle B(k \hat{e}_z; s_B) C(-k \hat{e}_z; s_C) | H_{sb}(0) | A(0; s_A) \rangle = (2\pi)^{3/2} \gamma_0 \int d^3 \mathbf{p} \varphi_B^*(\mathbf{p}) \varphi_C^*(\mathbf{p}) \varphi_A \left[\mathbf{p} + \frac{k}{2} \hat{e}_z \right] \sqrt{8 \tilde{M}_A \tilde{M}_B \tilde{M}_C} [\delta_{ab} \delta_{\bar{a}\bar{b}} \delta_{bc}^E \chi(s_c \bar{s}_b) - \delta_{ac} \delta_{\bar{a}\bar{b}} \delta_{cb}^E \chi(s_b \bar{s}_c)] (-1)^{L_A + L_B + L_C}, \quad (\text{B13})$$

where \tilde{M} denotes a mock mass,¹⁷ L denotes a quark-antiquark relative angular momentum, φ denotes a total wave function including spin, flavor, and spatial degrees of freedom, and γ_0 is the string-breaking constant. The notation is such that, for example, the indices a and \bar{a} denote the flavor and spin-projection onto the z axis for, respectively, the quark and antiquark of meson A . The symbol δ^F specifies that the Kronecker δ function is to be applied only to the flavor degrees of freedom. The function χ is given by $\chi(\uparrow; \uparrow) = -\chi^*(\downarrow; \downarrow) = 2p \sin\theta e^{-i\phi}$ and $\chi(\uparrow; \downarrow) = \chi(\downarrow; \uparrow) = k - 2p \cos\theta$ where p is the magnitude of \mathbf{p} and (θ, ϕ) are the polar angles specifying \mathbf{p} with respect to the z axis. We use simple harmonic-oscillator wave functions for computational simplicity. Calculations of the above matrix element utilizing such naive wave functions agree fairly well with those using more sophisticated wave functions in most cases.¹⁷

TABLE V. The strong decay on-shell form factors.

	Model prediction	Fit to data
$f_{\rho\pi\pi}(m_{\rho}^2)$	6.08 ^a	6.08±0.04
$f_{a\rho\pi}(m_{a_1}^2, m_{\rho}^2)$ (GeV)	4.8	4.6±0.2 ^b
$g_{a\rho\pi}(m_{a_1}^2, m_{\rho}^2)$ (GeV)	6.0	5.4±0.5 ^b
$f_{\pi'\rho\pi}(m_{\pi'}^2, m_{\rho}^2)$	5.8	—
$f_{aK^*K}(m_{a_1}^2, m_{K^*}^2)$ (GeV)	7.3	—
$g_{aK^*K}(m_{a_1}^2, m_{K^*}^2)$ (GeV)	11.9	—

^aFit to $\rho \rightarrow \pi\pi$ to determine string-breaking constant γ_0 .

^bFit to $\tau \rightarrow \nu_{\tau} \pi \pi \pi$ (Fig. 3) and $\pi\pi$ projections (Fig. 4).

The two form factors $f_{a\rho\pi}$ and $g_{a\rho\pi}$ can be related to the S - and D -wave amplitudes for $a_1 \rightarrow \rho\pi$. Defining

$$\langle \rho(\mathbf{k} s_{\rho}) \pi(-\mathbf{k}) | H_{sb}(0) | a_1(0 s_a) \rangle = i f_{a\rho\pi}^S \delta_{s_a s_{\rho}} Y_{00}(\Omega_k) + i f_{a\rho\pi}^D \sum_{m_L} C(211; m_L s_{\rho} s_a) Y_{2m_L}(\Omega_k), \quad (\text{B11})$$

where s_{ρ} and s_a are the spin projections along the z axis for the ρ and a_1 , one finds

$$f_{a\rho\pi}^S(m_{a_1}^2, m_{\rho}^2) = \frac{\sqrt{4\pi}}{3m_{\rho}} [(E_{\rho} + 2m_{\rho}) f_{a\rho\pi}(m_{a_1}^2, m_{\rho}^2) + \mathbf{k}^2 m_a g_{a\rho\pi}(m_{a_1}^2, m_{\rho}^2)], \quad (\text{B12})$$

$$f_{a\rho\pi}^D(m_{a_1}^2, m_{\rho}^2) = -\frac{\sqrt{8\pi}}{3m_{\rho}} [(E_{\rho} - m_{\rho}) f_{a\rho\pi}(m_{a_1}^2, m_{\rho}^2) + \mathbf{k}^2 m_a g_{a\rho\pi}(m_{a_1}^2, m_{\rho}^2)],$$

where $Y_{Lm_L}(\Omega)$ and $C(LSJ; m_L m_S m_J)$ are standard spherical harmonics and Clebsch-Gordan coefficients. Note that the association (see, e.g., Ref. 13) of $f_{a\rho\pi}$ with the S -wave decay amplitude is incorrect.

To compute the Lorentz-invariant form factors in the quark model, one first calculates the following matrix element for specific polarization states:

The form factors are then obtained by equating the above amplitudes to expressions (B8)–(B10) and replacing mass squares by the appropriate Dalitz-plot variables. The results are

$$f_{\rho\pi\pi}(s_i) = \frac{\sqrt{3}}{2} \kappa_{\rho\pi\pi} \left[\frac{\beta_\rho}{\beta_{\rho\pi\pi}^2} \right] (1 + \xi_{\rho\pi\pi}) F_{\rho\pi\pi}(\mathbf{p}_i^2), \quad (\text{B14})$$

$$f_{a\rho\pi}(s, s_i) = \frac{4}{\sqrt{3}} \kappa_{a\rho\pi} \left[1 - \frac{3\mathbf{k}_i^2}{8\beta_{a\rho\pi}^2} (1 - \xi_{a\rho\pi}^2) \right] F_{a\rho\pi}(\mathbf{k}_i^2), \quad (\text{B15})$$

$$g_{a\rho\pi}(s, s_i) = \frac{4}{\sqrt{3}} \kappa_{a\rho\pi} \frac{\sqrt{\mathbf{k}_i^2 + s_i}}{\sqrt{s} \mathbf{k}_i^2} \left[\left(\frac{s_i}{\mathbf{k}_i^2 + s_i} \right)^{1/2} - 1 + \frac{3\mathbf{k}_i^2}{8\beta_{a\rho\pi}^2} (1 - \xi_{a\rho\pi}^2) \right] F_{a\rho\pi}(\mathbf{k}_i^2), \quad (\text{B16})$$

$$f_{\pi'\rho\pi}(s, s_i) = \frac{1}{\sqrt{2}} \kappa_{\pi'\rho\pi} \left[\frac{\beta_{\pi'}}{\beta_{\pi'\rho\pi}^2} \right] \left[\frac{s_i}{s} \right]^{1/2} \left[(2\xi_{\pi'\rho\pi} + 1)(3 - 5\xi_{\pi'\rho\pi}) - \frac{\mathbf{k}_i^2}{2\beta_{\pi'}^2} (1 + \xi_{\pi'\rho\pi})(1 - \xi_{\pi'\rho\pi})^2 \right] F_{\pi'\rho\pi}(k_i^2), \quad (\text{B17})$$

where

$$F_{ABC}(\mathbf{k}_i^2) = \exp \left[-\frac{\mathbf{k}_i^2}{12} \left[\frac{\beta_{ABC}(\beta_B^2 + \beta_C^2)}{2\beta_A^2 \beta_B^2 \beta_C^2} \right] \right], \quad (\text{B18})$$

$$\kappa_{ABC} = \sqrt{8\bar{M}_A \bar{M}_B \bar{M}_C} \frac{8\gamma_0 \pi^{3/4}}{9\beta_{ABC}^{1/2}} \left[\frac{\beta_{ABC}}{\beta_A} \right]^{5/2} \left[\frac{\beta_{ABC}}{\beta_B \beta_C} \right]^{3/2}, \quad (\text{B19})$$

$$\xi_{ABC} = \beta_{ABC}^2 / (3\beta_A^2), \quad (\text{B20})$$

$$\beta_{ABC}^{-2} = \frac{1}{3}(\beta_A^{-2} + \beta_B^{-2} + \beta_C^{-2}), \quad (\text{B21})$$

$$\mathbf{k}_i^2 = [(s - s_i - m_\pi^2)^2 - 4m_\pi^2 s_i] / (4s), \quad (\text{B22})$$

$$\mathbf{p}_i^2 = \frac{s_i}{4} - m_\pi^2. \quad (\text{B23})$$

The form factors f_{aK^*K} and g_{aK^*K} are obtained by replacing ρ by K^* or \bar{K}^* and π by \bar{K} or K in the expressions for $f_{a\rho\pi}/\sqrt{2}$ and $g_{a\rho\pi}/\sqrt{2}$. Some numerical results are given in Table V. In our numerical results we take all $\beta_i = \beta$, with $\beta = 0.4$ GeV in our ‘‘preferred fit.’’¹⁷

¹See, for example, N. Isgur, in *Proceedings of the International School of Physics with Low Energy Antiprotons*, Erice, Italy, 1987, edited by U. Gastaldi (Plenum, New York, in press).

²The DELCO Collaboration, W. B. Ruckstuhl *et al.*, *Phys. Rev. Lett.* **56**, 2132 (1986).

³The Mark II Collaboration, W. B. Schmidke *et al.*, *Phys. Rev. Lett.* **57**, 527 (1986).

⁴The ARGUS Collaboration, H. Albrecht *et al.*, *Z. Phys. C* **33**, 7 (1986).

⁵The MAC Collaboration, H. R. Band *et al.*, *Phys. Lett. B* **198**, 297 (1987).

⁶C. Daum *et al.*, *Nucl. Phys.* **B182**, 269 (1981).

⁷J. Dankowych *et al.*, *Phys. Rev. Lett.* **46**, 580 (1981).

⁸R. T. Deck, *Phys. Rev. Lett.* **13**, 169 (1964).

⁹Particle Data Group, *Phys. Lett.* **170B**, 1 (1986).

¹⁰M. G. Bowler, *Phys. Lett. B* **182**, 400 (1986).

¹¹There are occasions on which general principles such as gauge or chiral invariance dictate that graphs other than the non-Z graph must contribute; so far as we are aware, this is not one of them.

¹²In most of the experimental analyses listed in Table I, the stronger assumption that only f_1 is nonzero was made. The form factors f_3 , f_4 , f_5 , and g_2 have been more or less universally ignored; see Refs. 13–16.

¹³W. R. Fraser, J. R. Fulco, and F. R. Halpern, *Phys. Rev.* **136**, B1207 (1964).

¹⁴G. Dillon and M. M. Giannini, *Nuovo Cimento* **54A**, 937 (1968).

¹⁵H. Kuhn and F. Wagner, *Nucl. Phys.* **B236**, 16 (1984).

¹⁶B. J. Read, *Nucl. Phys.* **B64**, 511 (1973); H. E. Haber and G. L. Kane, *ibid.* **B129**, 429 (1977).

¹⁷R. Kokoski and N. Isgur, *Phys. Rev. D* **35**, 907 (1987).

¹⁸The flux-tube-breaking model of Ref. 17 is for many purposes, including those of this paper, very similar in its consequences to the 3P_0 quark-pair-creation model. See, for the latter, A. Le Yaouanc, L. Oliver, O. Pène, and J. C. Raynal, *Phys. Rev. D* **8**, 2223 (1973); **9**, 1415 (1974); **11**, 1272 (1975); M. Chaichan and R. Kogerler, *Ann. Phys. (N.Y.)* **124**, 61 (1980).

¹⁹N. A. Törnqvist, *Z. Phys. C* **36**, 695 (1987); **40**, 632E (1988).

We thank the author for several useful conversations on the relationship of his work to ours.

²⁰It should be noted that the hadronic reactions were fit with a far less elaborate a_1 .

²¹S. Godfrey and N. Isgur, *Phys. Rev. D* **32**, 189 (1985).

²²C. Hayne and N. Isgur, *Phys. Rev. D* **25**, 1944 (1982); for a more recent version of this calculation, see Ref. 21.

²³S. Weinberg, *Phys. Rev. Lett.* **18**, 507 (1967); H. J. Schnitzer and S. Weinberg, *Phys. Rev.* **164**, 1828 (1967).